

MAGNETOCENTRIFUGALLY DRIVEN WINDS: COMPARISON OF MHD SIMULATIONS WITH THEORY

G. V. USTYUGOVA

Keldysh Institute of Applied Mathematics, Russian Academy of Sciences, Moscow, Russia, 125047; ustyugg@spp.Keldysh.ru

A. V. KOLDOBA

Institute of Mathematical Modeling, Russian Academy of Sciences, Moscow, Russia, 125047

M. M. ROMANOVA

Space Research Institute, Russian Academy of Sciences, Moscow, Russia; and Department of Astronomy, Cornell University, Ithaca, NY 14853-6801; romanova@astrosun.tn.cornell.edu

V. M. CHECHETKIN

Keldysh Institute of Applied Mathematics, Russian Academy of Sciences, Moscow, Russia; chech@spp.Keldysh.ru

AND

R. V. E. LOVELACE

Department of Astronomy, Cornell University, Ithaca, NY 14853-6801; rv11@cornell.edu

Received 1998 July 1; accepted 1998 December 7

ABSTRACT

Stationary MHD outflows from a rotating accretion disk are investigated numerically by time-dependent axisymmetric simulations. The initial magnetic field is taken to be a split-monopole poloidal field configuration frozen into the disk. The disk is treated as a perfectly conducting, time-independent density boundary $[\rho(r)]$ in Keplerian rotation. The outflow velocity from this surface is not specified but rather is determined self-consistently from the MHD equations. The temperature of the matter outflowing from the disk is small in the region where the magnetic field is inclined away from the symmetry axis ($c_s^2 \ll v_K^2$) but relatively high ($c_s^2 \lesssim v_K^2$) at very small radii in the disk, where the magnetic field is not inclined away from the axis. We have found a large class of stationary MHD winds. Within the simulation region, the outflow accelerates from thermal velocity ($\sim c_s$) to a much larger asymptotic poloidal flow velocity of the order of $\frac{1}{2}\sqrt{GM/r_i}$, where M is the mass of the central object and r_i is the inner radius of the disk. This asymptotic velocity is much larger than the local escape speed and is larger than fast magnetosonic speed by a factor of ~ 1.75 . The *acceleration distance* for the outflow, over which the flow accelerates from $\sim 0\%$ to, say, 90% of the asymptotic speed, occurs at a flow distance of about $80r_i$. The outflows are approximately spherical, with only small collimation within the simulation region. The *collimation distance* over which the flow becomes collimated (with divergence less than, say, 10^0) is much larger than the size of our simulation region. Close to the disk the outflow is driven by the centrifugal force, while at all larger distances the flow is driven by the magnetic force, which is proportional to $-\nabla(rB_\phi)^2$, where B_ϕ is the toroidal field. Our stationary numerical solutions allow us to (1) compare the results with MHD theory of stationary flows, (2) investigate the influence of different outer boundary conditions on the flows, and (3) investigate the influence of the shape of the simulation region on the flows. Different comparisons were made with the theory. The ideal MHD integrals of motion (constants on flux surfaces) were calculated along magnetic field lines and were shown to be constants with an accuracy of 5% – 15% . Other characteristics of the numerical solutions were compared with the theory, including conditions at the Alfvén surface. Different outer boundary conditions on the toroidal component of the magnetic field were investigated. We conclude that the commonly used “free” boundary condition on the toroidal field leads to artificial magnetic forces on the outer boundaries, which can significantly influence to the calculated flows. New outer boundary conditions are proposed and investigated that do not give artificial forces. We show that simulated flows may depend on the shape of the simulation region. Namely, if the simulation region is elongated in the z -direction, then Mach cones on the outer cylindrical boundary may be partially directed inside the simulation region. Because of this, the boundary can have an artificial influence on the calculated flow. This effect is reduced if the computational region is approximately square or if it is spherical. Simulations of MHD outflows with an elongated computational region can lead to *artificial* collimation of the flow.

Subject headings: accretion, accretion disks — galaxies: jets — ISM: jets and outflows — ISM: magnetic fields — MHD — plasmas

1. INTRODUCTION

The existence and nature of MHD outflows from an accretion disk threaded by an ordered magnetic field is a long-standing astrophysical problem. The problem has been investigated theoretically by many authors (Blandford & Payne 1982; Pudritz & Norman 1986; Sakurai 1987; Kou-

pelis & Van Horn 1989; Lovelace, Berk, & Contopoulos 1991; Pelletier & Pudritz 1992; Königl & Ruden 1993; Cao & Spruit 1994; Contopoulos & Lovelace 1994; Contopoulos 1995; Ostriker 1997). See also reviews by Bisnovatyi-Kogan (1993) and Livio (1997). From the theory, a necessary condition for magnetically/centrifugally

driven outflows is that the poloidal magnetic field at the disk's surface be inclined away from the symmetry axis (z) at a sufficiently large angle.

However, the analytical theory makes drastic simplifications, such as assuming self-similar dependences on the radial distance (r in cylindrical coordinates) or integrating over the cross section of the outflow. The self-similar solutions have divergences at both small and large r so that the influence of these regions is unknown.

Numerical MHD simulations are essential to establish the existence and understand the nature of magnetically/centrifugally driven outflows. Stationary and nonstationary MHD flows were investigated by Kudoh & Shibata (1995, 1997a, 1997b) in one-dimensional (1.5 D) simulations. These simulations allowed an investigation of outflows for a wide range of parameters. However, they supposed a fixed configuration of the poloidal magnetic field. Two-dimensional (2.5 D) simulations of outflows from accretion disks were performed by Uchida & Shibata (1985), Shibata & Uchida (1986), Stone & Norman (1994), and Matsumoto et al. (1996). These simulations led to strongly nonstationary accretion and outflows from the disk. In most of these studies the nonstationarity of the solutions is due to the start-up conditions with the disk rotating but the corona of the disk not rotating. In other cases the nonstationarity is due to the disk rotating at a significantly sub-Keplerian rate. These simulations are valuable in showing that temporary MHD outflows are possible, but the results depend strongly on the assumed initial conditions.

In order to avoid the strong dependence on initial conditions and the problems associated with following the internal dynamics of the accretion disk, we earlier proposed treating the outer surface layers of the disk as a boundary condition (Ustyugova et al. 1995; Koldoba et al. 1996; Romanova et al. 1997, 1998). This approach has been followed by others (Ouyed & Pudritz 1997; Ouyed, Pudritz, & Stone 1997; Meier et al. 1997). In these simulations the "disk" represents an outer layer of the accretion disk. In the actual situation, the outflowing matter will affect the disk evolution, or at least the evolution of the surface layers of the disk. The angular momentum carried away by MHD outflows can give a disk accretion rate that is much larger than the viscous accretion rate of say an α -disk, but the accretion speeds are typically much smaller than the free-fall speed (Lovelace, Romanova, & Newman 1994; Lovelace, Newman, & Romanova 1997). Thus the disk can be treated as stationary during the formation and establishment of MHD outflows, which takes place on a free-fall timescale. However, the long-time simulations of outflows, including the back reaction on the disk, are clearly of interest for future research.

Different initial magnetic field configurations have been assumed in earlier studies. The initial field assumed by Ouyed & Pudritz (1997) was the Cao & Spruit (1994) field, which decreases slowly with radial distance on the disk's surface. On the other hand, the initial magnetic field of Ustyugova et al. (1995) was the split-monopole field (Sakurai 1987, 1985), which decreases rapidly with radial distance on the disk surface. The temperature of matter outflowing from the disk of Ouyed & Pudritz (1997) was small, and the initial magnetic field was weak. However, Ouyed & Pudritz (1997) introduced a spectrum of turbulent Alfvén waves with a high pressure, which is similar to having a high-temperature corona. Thus the approach of

Ouyed & Pudritz (1997) is similar to that of Ustyugova et al. (1995), where the magnetic field is weak and the coronal temperature is high. In both papers, the initial twist of the magnetic field results from the disk rotation, because the corona is not rotating. This twisting of the magnetic field gives the collimation observed in both papers.

It is important to get stationary outflows using time-dependent MHD equations because the nonstationary flows may be artifacts of the initial conditions. Stationary, magnetocentrifugally driven outflows for relatively low temperature of the "disk" matter were obtained in the 2.5 D simulations by Romanova et al. (1997) for the case where the initial magnetic field was a "tapered" split-monopole-type field. This work found that in the stationary state the outflow was quasi-spherical, with essentially no collimation within the simulation region. Close to the disk the outflow was driven by the centrifugal force, while at larger distances the magnetic force was dominant.

In this work we investigate the case of a pure (that is, nontapered) split-monopole magnetic field by axisymmetric (2.5 D) numerical simulations. The motivation was to study MHD outflows from a relatively cold accretion disk where magnetic field lines are inclined away from the symmetry axis. To remove the influence of the region near the axis where magnetic field lines are not significantly inclined, we pushed hot matter from the disk in the small area around the axis. We compare our simulation results with the theory of stationary MHD flows. Furthermore, we use our stationary simulation flows to investigate the influence of outer-boundary conditions. Our earlier study (Romanova et al. 1997) showed that some simple outer-boundary conditions on the toroidal magnetic field can lead to artificial forces on the boundary that significantly influence the flow within the simulation region. Here we consider in further detail the influence of outer-boundary conditions on the calculated flows.

In § 2 the theory of stationary MHD flows is briefly reviewed. In § 3 the numerical model is presented. The influence of the outer boundary condition on the toroidal magnetic field and the shape of the computational region is analyzed in § 4. In § 5 we present results of simulations of stationary flows and compare them with theory. In § 6 the conclusions of this work are summarized.

2. THEORY OF STATIONARY MHD FLOWS

The theory of stationary, axisymmetric, ideal MHD flows was developed by Chandrasekhar (1956), Woltjer (1959), Mestel (1961, 1968), Kulikovskiy & Lyubimov (1962), and others. Under these conditions the MHD equations can be reduced to a single equation for the "flux function," $\Psi(r, z)$, in cylindrical (r, ϕ, z) coordinates (Heinemann & Olbert 1978; Lovelace et al. 1986). The flux function, Ψ , labels flux surfaces so that $\Psi(r, z) = \text{constant}$ represents the poloidal projection of a field line. The equation for Ψ is commonly referred to as the Grad-Shafranov equation (Lovelace et al. 1986).

2.1. Integrals of Motion

For axisymmetric conditions the flow field can be written as $\mathbf{v} = \mathbf{v}_p + v_\phi \mathbf{e}_\phi$, where \mathbf{v}_p is the poloidal (r, z) component, $v_\phi = \omega r > 0$ is the toroidal component, and \mathbf{e}_ϕ is the unit toroidal vector. Similarly, the magnetic field can be written as $\mathbf{B} = \mathbf{B}_p + B_\phi \mathbf{e}_\phi$. The ideal MHD equations then imply that certain quantities are constants on any given flux

surface $\Psi(r, z) = \text{constant}$, or, equivalently, they are constants along any given stream line or a given magnetic field line. These integrals are functions of Ψ (see, e.g., Lovelace et al. 1986):

$$\mathbf{v}_p = \frac{K(\Psi)}{4\pi\rho} \mathbf{B}_p, \quad (1)$$

$$\omega r^2 - \frac{rB_\phi}{K} = \Lambda(\Psi), \quad (2)$$

$$\omega - \frac{KB_\phi}{4\pi\rho r} = \Omega(\Psi), \quad (3)$$

$$S = S(\Psi), \quad (4)$$

$$w + \Phi - \frac{\Omega^2 r^2}{2} + \frac{v_p^2}{2} + \frac{1}{2}(\omega - \Omega)^2 r^2 = E(\Psi). \quad (5)$$

Here S is the entropy, w is the enthalpy, and Φ is the gravitational potential. The quantity K corresponds to the conservation of mass along a streamline, Λ to the conservation of angular momentum, Ω to the conservation of helicity, S to the conservation of entropy, and E (Bernoulli's constant) to the conservation of energy.

The remaining MHD equation (which cannot be written in the integral form) is the Euler force equation across the poloidal magnetic field line (Bogovalov 1997),

$$\begin{aligned} & (v_p^2 - v_{Ap}^2) \frac{\partial \theta}{\partial s} - \frac{\cos \theta}{r} (v_\phi^2 - v_{A\phi}^2) \\ & + \frac{1}{\rho} \frac{\partial}{\partial n} \left(p + \frac{\mathbf{B}^2}{8\pi} \right) + \frac{\partial \Phi}{\partial n} = 0, \end{aligned} \quad (6)$$

which is equivalent to the Grad-Shafranov equation. Here $\partial/\partial n$ is the derivative in the direction perpendicular to magnetic field lines and directed outward from the axis, θ is the angle of inclination of the poloidal magnetic field line away from the z -axis, s is the distance from the disk along a magnetic field line, and $v_{Ap} \equiv |\mathbf{B}_p|/\sqrt{4\pi\rho}$ and $v_{A\phi} \equiv |B_\phi|/\sqrt{4\pi\rho}$ are the poloidal and azimuthal Alfvén velocities. The quantity $\partial\theta/\partial s$ is the curvature of magnetic field line. The first two terms in equation (6) are determined by the nondiagonal (tension) part of the stress tensor, $\rho v_i v_k + (p + \mathbf{B}^2/8\pi)\delta_{ik} - B_i B_k/4\pi$. The third term is determined by the total (matter plus magnetic) pressure $p + \mathbf{B}^2/8\pi$ and the gravity force $\partial\Phi/\partial n$.

2.2. Physical Sense of Integrals of Motion

To clarify the physical sense of the integrals of motion, it is useful to derive the fluxes of mass, angular momentum (about the z -axis), and energy. The corresponding conservation laws for stationary conditions are

$$\nabla \cdot (\rho \mathbf{v}_p) = 0, \quad (7)$$

$$\nabla \cdot \left(r \rho \mathbf{v}_p v_\phi - \frac{\mathbf{B}_p r B_\phi}{4\pi} \right) = 0, \quad (8)$$

$$\nabla \cdot \left[\rho \mathbf{v}_p \left(\frac{v^2}{2} + \frac{\mathbf{B}^2}{4\pi\rho} + w + \Phi \right) - \frac{\mathbf{B}_p (\mathbf{v} \cdot \mathbf{B})}{4\pi} \right] = 0. \quad (9)$$

Because $\mathbf{v}_p \parallel \mathbf{B}_p$, the vector flux densities are directed along the field lines.

Consider the fluxes through an annular region with surface area element dS . The matter flux through the axisymmetric surface S extending out from the z -axis is

$$\mathcal{F}_M = \int_S dS \cdot \rho \mathbf{v}_p = \frac{1}{4\pi} \int_S dS \cdot \mathbf{B}_p K(\Psi), \quad (10)$$

where we took into account the integral (eq. [1]). $dS \cdot \mathbf{B}_p$ is the magnetic flux through the annular region bounded by flux surfaces Ψ and $\Psi + d\Psi$. Thus we can change from space integration to integration over Ψ . Because $B_r = -(1/r)\partial\Psi/\partial z$ and $B_z = (1/r)\partial\Psi/\partial r$, we have

$$\mathcal{F}_M(\Psi) = \frac{1}{2} \int_0^\Psi d\Psi' K(\Psi'), \quad (11)$$

where $\Psi = 0$ corresponds to the z -axis. Similarly,

$$\begin{aligned} \mathcal{F}_L(\Psi) &= \int dS \cdot \left(r \rho \mathbf{v}_p v_\phi - \frac{\mathbf{B}_p r B_\phi}{4\pi} \right) \\ &= \frac{1}{2} \int_0^\Psi d\Psi' \Lambda(\Psi') K(\Psi'), \end{aligned} \quad (12)$$

$$\begin{aligned} \mathcal{F}_E(\Psi) &= \int dS \cdot \rho \mathbf{v}_p \left[\left(\frac{v^2}{2} + \frac{\mathbf{B}^2}{4\pi\rho} + w + \Phi \right) - \frac{\mathbf{B}_p \mathbf{v} \cdot \mathbf{B}}{4\pi} \right] \\ &= \frac{1}{2} \int_0^\Psi d\Psi' (E + \Lambda\Omega) K. \end{aligned} \quad (13)$$

Thus $Kd\Psi/2$ is the matter flux between the flux surfaces separated by $d\Psi$, $\Lambda Kd\Psi/2$ is the angular momentum flux, and $(E + \Lambda\Omega)Kd\Psi/2$ is the energy flux. Note that $\Lambda(\Psi)$ is the specific angular momentum carried along the magnetic field line $\Psi = \text{constant}$, $E(\Psi) + \Lambda\Omega(\Psi)$ is the specific energy, and $\Omega(\Psi)$ is the angular velocity of the disk at the point where the magnetic field line or flux surface, $\Psi = \text{constant}$, intersects the disk (for $|v_p| \rightarrow 0$ at the disk).

2.3. Conditions at the Alfvén Surface

Conditions at the Alfvén surface are known to be important for the global properties of MHD flows (Weber & Davis 1967). Equations (2) and (3) constitute a linear system of equations for ω and B_ϕ . The determinant of this system is zero if $K^2 = 4\pi\rho$. Under this condition a solution exists if $\Lambda = r^2\Omega$ (Weber & Davis 1967), which corresponds to $\mathbf{v}_p = \mathbf{B}_p/\sqrt{4\pi\rho} = \mathbf{v}_{Ap}$. This is the condition that defines the Alfvén surface. Figure 1 shows a possible field line $\Psi = \text{constant}$ and Alfvén surface A . The radius at which this field line intersects the disk is $r_d(\Psi)$. The radius at which it crosses the Alfvén surface is $r_A(\Psi)$. The density at this point on the Alfvén surface is $\rho_A(\Psi)$. Thus

$$\rho_A(\Psi) = K^2(\Psi)/4\pi, \quad r_A^2(\Psi) = \Lambda(\Psi)/\Omega(\Psi). \quad (14)$$

Equations (2) and (3) give

$$\omega = \Omega \frac{1 - \rho_A r_A^2 / \rho r^2}{1 - \rho_A / \rho}, \quad (15)$$

$$B_\phi = r\Omega \sqrt{4\pi\rho_A} \frac{1 - r_A^2 / r^2}{1 - \rho_A / \rho}. \quad (16)$$

Taking into account (14)–(16), one can express the fluxes of mass, angular momentum, and energy, using only the

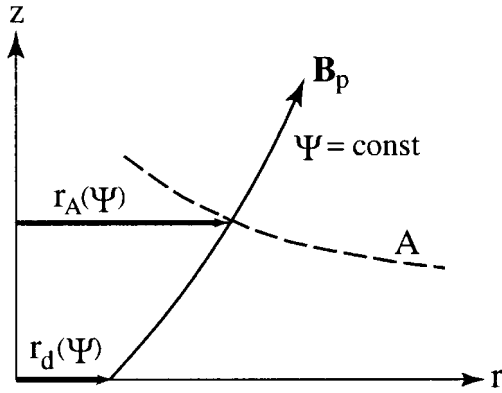


FIG. 1.—Poloidal magnetic field line $\Psi = \text{const}$ (solid line) that starts at the radial distance $r = r_d(\Psi)$ on the disk and crosses the Alfvén surface A (dashed line) at the radial distance $r_A(\Psi)$ from the axis.

values of physical quantities on the Alfvén surface:

$$\mathcal{F}_M(\Psi) = \int_0^\Psi d\Psi' \sqrt{\pi\rho_A}, \quad (17)$$

$$\mathcal{F}_L(\Psi) = \int_0^\Psi d\Psi' \sqrt{\pi\rho_A} \Omega r_A^2, \quad (18)$$

$$\mathcal{F}_E(\Psi) = \int_0^\Psi d\Psi' \sqrt{\pi\rho_A} (E + \Omega^2 r_A^2). \quad (19)$$

2.4. Forces

For understanding the plasma acceleration, we project the different forces onto the poloidal magnetic field lines. As was mentioned, in a stationary state, matter flows along the poloidal magnetic field lines. The acceleration in the poloidal (r, z) plane is

$$(\mathbf{v}_p \cdot \nabla) \mathbf{v}_p + v_\phi (\mathbf{e}_\phi \cdot \nabla) (v_\phi \mathbf{e}_\phi). \quad (20)$$

The last term represents the centrifugal acceleration $-(v_\phi^2/r)\mathbf{e}_r = -r\omega^2\mathbf{e}_r$. To get the force per unit mass along a magnetic field line, we multiply the Euler equation by a unit vector, $\hat{\mathbf{b}}$, parallel to \mathbf{B}_p . This gives

$$f = \omega^2 r \sin \theta - \frac{1}{\rho} \frac{\partial p}{\partial s} - \frac{\partial \Phi}{\partial s} + \frac{1}{4\pi\rho} \hat{\mathbf{b}} \cdot [(\nabla \times \mathbf{B}) \times \mathbf{B}], \quad (21)$$

where θ is the inclination angle of the field line to the z -axis. The final term of equation (21) is the projection of the magnetic force in the direction of $\hat{\mathbf{b}}$, which can be transformed to

$$f_M = \frac{1}{4\pi\rho} \hat{\mathbf{b}} \cdot [(\nabla \times \mathbf{B}) \times \mathbf{B}] = -\frac{1}{8\pi\rho r^2} \frac{\partial (rB_\phi)^2}{\partial s},$$

which is useful for understanding our results.

When magnetic field lines are inclined outward, away from the symmetry axis, the gravitational force $f_G = \partial\Phi/\partial s$ opposes the outflow of matter from the disk. If the matter is relatively cold, then the pressure gradient force $f_p = -(1/\rho)(\partial p/\partial s)$ is unimportant. Then matter can be accelerated outward by the centrifugal force $f_C = \omega^2 r \sin \theta$ and/or the magnetic force f_M . This determines the driving mechanisms of the outflow, centrifugal and/or magnetic. The centrifugal force always acts to accelerates matter outward if the distance between magnetic field line and the axis increases. Consider the direction of the magnetic force.

Note that the lines on which $rB_\phi = \text{constant}$ are also poloidal current-density lines; that is, $\mathbf{j}_p = -(\mathbf{e}_\phi/r) \times \nabla(rB_\phi)$ so that $\mathbf{j}_p \cdot \nabla(rB_\phi) = 0$. Consider a configuration of magnetic field line $\Psi = \text{constant}$ and a line of current-density \mathbf{j}_p , as is shown in Figure 2. The poloidal component of the magnetic force, $\propto -\nabla(rB_\phi)^2$, is perpendicular to the current-density \mathbf{j}_p and is shown in Figure 2 by arrows. Projection of this force onto the poloidal magnetic field shows that the force pushes matter upward near the disk (lower part of the region) and pushes matter downward farther from the disk (upper part of the region). The ϕ -component of the magnetic force $\propto \mathbf{j}_p \times \mathbf{B}_p$ acts in the direction of the disk rotation and leads to winding of the magnetic field line close to the disk and unwinding of magnetic field line farther from the disk.

Thus magnetic and centrifugal forces may both accelerate matter, but this depends on the configuration of magnetic field and current-density lines.

2.5. Collimation

Consider now the collimation of the flow. From equation (6), taking into account that $\cos \theta = \partial r/\partial n$, we have

$$(\mathbf{v}_p^2 - v_{Ap}^2) \frac{\partial \theta}{\partial s} = -\frac{1}{8\pi\rho r^2} \frac{\partial}{\partial n} (rB_\phi)^2 + \frac{\cos \theta v_\phi^2}{r} - \frac{1}{\rho} \frac{\partial}{\partial n} \left(p + \frac{B_p^2}{8\pi} \right) - \frac{\partial \Phi}{\partial n}. \quad (22)$$

At large distances from the Alfvén surface $r \gg r_A$, the density $\rho \ll \rho_A$, but values ρr^2 and v_p^2 remain finite (Heyvaerts & Norman 1989). Then $v_{Ap}^2 = (\rho/\rho_A)^2 v_p^2 \ll v_p^2$ so that the second term on the left-hand side of equation (22) is negligible. On the right-hand side, only the first term is important for $r \gg r_A$. Then equation (22) simplifies to

$$v_p^2 \frac{\partial \theta}{\partial s} = -\frac{1}{8\pi\rho r^2} \frac{\partial}{\partial n} (rB_\phi)^2. \quad (23)$$

Thus the curvature of magnetic field lines in the region $r \gg r_A$ is determined by the gradient $(rB_\phi)^2$. Figure 3 shows

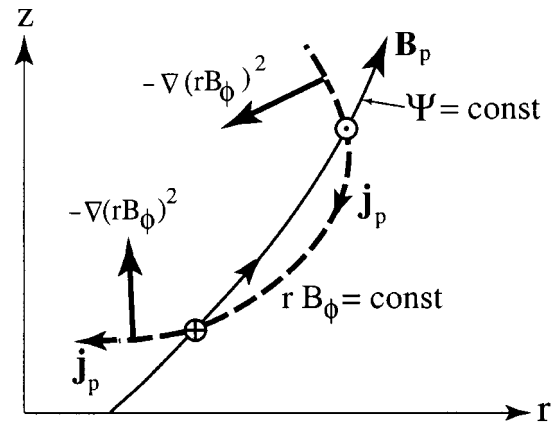


FIG. 2.—Directions of the magnetic forces for different configurations of the poloidal magnetic field \mathbf{B}_p (solid line) and the poloidal current-density \mathbf{j}_p (dashed line). The magnetic force in the poloidal plane $\propto -\nabla(rB_\phi)^2$ is perpendicular to the poloidal current density. The lower part of the figure shows the case where the magnetic force pushes matter away from the disk, while the top part of the figure shows the opposite situation. The force in the azimuthal direction $\mathbf{j}_p \times \mathbf{B}_p/c$ acts in the direction of rotation of the disk in the bottom part of the figure and in opposite direction in the top part.

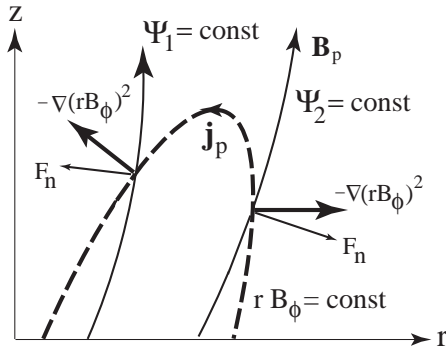


FIG. 3.—Poloidal current-density line j_p on which $rB_\phi = \text{constant}$ and two poloidal field lines. On the field line Ψ_1 , the magnetic force $\propto -\nabla(rB_\phi)^2$ acts to give collimation, while for the field line Ψ_2 the force acts to “anticollimate” the flow.

examples where two magnetic field lines Ψ_1 and Ψ_2 cross the line $rB_\phi = \text{constant}$. Again, the magnetic force $\propto -\nabla(rB_\phi)^2$ acts in the direction perpendicular to the current-density j_p . Here we are interested in the projection of this force onto a poloidal magnetic field line. From the figure one can see that the magnetic force acts to “collimate” the magnetic field line Ψ_1 and “anticollimate” the field line Ψ_2 .

3. NUMERICAL SIMULATIONS OF MHD OUTFLOWS

For our time-dependent simulations of axisymmetric flows of an ideal plasma in a gravitational field, the equations are

$$\frac{\partial \rho}{\partial t} + \nabla \cdot (\rho \mathbf{v}) = 0, \quad (24)$$

$$\frac{\partial(\rho \mathbf{v})}{\partial t} + \nabla \cdot \mathcal{T} = \rho \mathbf{g}, \quad (25)$$

$$\frac{\partial \mathbf{B}}{\partial t} - \nabla \times (\mathbf{v} \times \mathbf{B}) = 0, \quad (26)$$

$$\frac{\partial(\rho S)}{\partial t} + \nabla \cdot (\rho \mathbf{v} S) = 0. \quad (27)$$

Here S is entropy, $\mathcal{T}_{jk} = \rho v_j v_k + p \delta_{jk} + (\mathbf{B}^2 \delta_{jk}/2 - B_j B_k)/(4\pi)$ is the stress tensor, $\mathbf{g} = -\nabla \Phi$ is the gravitational acceleration, and Φ is the gravitational potential of the central object.

The energy equation (eq. [27]) is written in conservative form. From equations (24) and (27), one also has

$$\frac{\partial[\rho f(S)]}{\partial t} + \nabla \cdot [\rho f(S) \mathbf{v}] = 0 \quad (28)$$

for any continuous function $f(S)$. We take the equation of state to be $p = (\gamma - 1)\rho e$, where e is specific internal energy and $\gamma = \text{constant}$. In the present work, $\gamma = 5/3$. We take $f(S) = p/\rho^\gamma$, because the right-hand side depends only on the entropy. We solve the system of equations (24)–(26) and (28) numerically.

The central object of mass M is at the center of our coordinate system. The disk is located at $z = 0$ and is

treated as a perfectly conducting surface rotating with Keplerian velocity $v_K(r)$. The gravitational acceleration \mathbf{g} diverges as $r \rightarrow 0$, but of course the presence of a star or black hole changes this dependence. Instead of including the finite size of the central object, the gravitational potential is smoothed close to the origin, $\Phi = -GM/(r^2 + z^2 + r_i^2)^{1/2}$, where r_i is the smoothing radius. The value r_i is always much smaller than the size of the computational region. For this smoothed potential, the Keplerian velocity (for $z = 0$) becomes $v_K = r\sqrt{GM/(r^2 + r_i^2)^{3/4}}$. Our results do not depend significantly on r_i , because the main part of the outflow occurs from the inclined magnetic field in the region of the disk where $r \gg r_i$.

3.1. Numerical Method

Equations (24)–(26) and (28) were solved with our Godunov-type numerical code (Koldoba, Kuznetsov, & Ustyugova 1992; Koldoba & Ustyugova 1994; Ustyugova et al. 1995). The code is based on the ideas of Roe (1986) for hydrodynamics and the related ideas of Brio & Wu (1988) for MHD. This type of total variation diminishing, numerical scheme has also been developed and investigated by others (e.g., Ryu, Jones, & Frank 1995). The code has passed a number of essential tests (Koldoba et al. 1992; Koldoba & Ustyugova 1994) that are analogous to those described by Ryu et al. (1995). Compared with our earlier applications of this code (Ustyugova et al. 1995; Koldoba et al. 1995), a number of improvements have been made, including a procedure for guaranteeing that $\nabla \cdot \mathbf{B} = 0$. To satisfy the condition $\nabla \cdot \mathbf{B} = 0$, we projected the calculated magnetic field to the subspace of solenoidal functions $\tilde{\mathbf{B}}$ at each time step. We introduced the function Ψ , which satisfies the equation

$$\left[r \frac{\partial}{\partial r} \left(\frac{1}{r} \frac{\partial}{\partial r} \right) + \frac{\partial^2}{\partial z^2} \right] \Psi = -r \left(\frac{\partial B_r}{\partial z} - \frac{\partial B_z}{\partial r} \right).$$

Then the magnetic field $\tilde{\mathbf{B}}$ was calculated for which $\nabla \cdot \tilde{\mathbf{B}} = 0$. A similar method was used by Ryu et al. (1995).

Most of the simulations were done on a grid with $N_r \times N_z$ points in cylindrical coordinates. For the calculations on an approximately square region we used an inhomogeneous grid with 100×100 points, while for the axially elongated region we used a homogeneous grid with 50×200 points. We also did a smaller number of simulations using spherical coordinates (R, θ, ϕ) and a grid $N_R \times N_\theta = 100 \times 50$.

3.2. Initial Conditions

The motivation for this work was the study of stationary MHD flows. Hence it may appear that the initial conditions are unimportant. However, in practice, an unfavorable choice of initial conditions can lead to an essentially longer stage of transition to stationary state, or, even worse, stationary flows may never be reached. The region right above the disk is the most important, because the velocity distribution near the disk determines the number of boundary conditions (the flow may be subsonic or supersonic). Also, the physical parameters, such as density and magnetic field, are largest just above the disk. Hence we worked more carefully on the equilibrium at small values of z . At large z , approximate equilibrium in the z -direction was sufficient, because the magnetic field, which is dominant in the corona,

stabilizes matter against the violent movements. The expressions given below are found to be useful initial conditions that give a smooth start-up of the outflows.

The initial conditions are arranged as follows. The disk and corona are considered to be threaded by a poloidal magnetic field of monopole type (Sakurai 1987), $\mathbf{B}_p = Q(\mathbf{R} - \mathbf{R}_Q)/|\mathbf{R} - \mathbf{R}_Q|^3$, where $Q = B_0 h^2$ is the ‘‘charge’’ of the monopole and \mathbf{R}_Q is the position vector of the monopole located on the symmetry axis at a distance h below the disk.

The temperature on the disk surface, which is proportional to the square of (isothermal) sound speed $c_T^2 = p/\rho$, was taken to have the dependence

$$c_T^2 = \Phi(r,0)(\kappa + \kappa_* e^{-r^2/r_T^2}), \quad (29)$$

where κ and κ_* are parameters, r_T is a characteristic radius inside of which the disk is relatively hot. For specificity we take $r_T = 2r_i$. For $r \gg r_T$, $c_T^2/\Phi(r,0) \approx \kappa$; that is, the sound speed is a constant fraction of the Keplerian velocity in the region where we expect centrifugally/magnetically driven outflows from the disk. The term in equation (29) with κ_* increases the temperature in the region near the axis, where magnetic or centrifugal outflows are not expected. For actual conditions, this part of the flow may be connected with the star or black hole (Livio 1997).

We supposed that the initial temperature of the corona is a function only of r , so that equation (29) is the initial condition for the entire computational region. Also, we supposed that in z -direction the gravitational force is balanced by the pressure gradient,

$$\frac{1}{\rho} \frac{\partial p}{\partial z} = \frac{c_T^2(r)}{\rho} \frac{\partial \rho}{\partial z} = -\frac{\partial \Phi}{\partial z}. \quad (30)$$

The solution of this equation is

$$p(r, z) = p_d(r) \exp \left[\frac{\Phi(r,0) - \Phi(r, z)}{c_T^2} \right], \quad (31)$$

where $p_d(r)$ is the pressure on the disk surface and $\Phi(r, 0)$ is the gravitational potential on the disk.

In the initial state, the surface of the disk is in equilibrium. We suppose that the gravitational force on the disk surface is compensated by the centrifugal force, while the matter pressure gradient in the r -direction is compensated by the magnetic force. That is, on the disk ($z = 0$),

$$\frac{\partial p_d}{\partial r} + \frac{1}{8\pi r^2} \frac{\partial (rB_\phi)^2}{\partial r} = 0. \quad (32)$$

The solution of this equation for pressure on the disk $p_d(r)$ and current $I_d(r) = (c/2)rB_\phi|_{z=0}$ flowing through a circular area of radius r on the disk can be written as

$$p_d(r) = \frac{B_0^2}{8\pi} \cos^n \theta, \quad (33)$$

$$I_d(r) = \frac{cB_0 h}{2} \left[\frac{n}{n-2} (1 - \cos^{n-2} \theta) - (1 - \cos^n \theta) \right]^{1/2}, \quad (34)$$

where $\cos \theta = h/(h^2 + r^2)^{1/2}$, with $h = \text{constant}$, and θ is the inclination of magnetic field line to the axis of rotation. This gave us possibility to find initial azimuthal magnetic field

along the disk, $B_\phi(r) = 2I_d(r)/cr$. Close to the disk, rB_ϕ is approximately constant along a magnetic field line. The three components of the initial magnetic field on the disk are shown in Figure 4.

To escape rapid twisting of the magnetic field due to the difference between the azimuthal velocities of the disk and the corona, we supposed that the corona initially rotates with an angular velocity that is constant on cylinders $r = \text{constant}$ and equal to v_K/r of the disk. As a result of this rotation, the corona is not in equilibrium in the r -direction. However, this lack of initial equilibrium does not disrupt the evolution of outflows from the disk, and it does not affect the final stationary states where the flow reaches equilibrium.

3.3. Boundary Conditions

The lower boundary of our simulation region is the disk that is perfectly conducting and rotates at the Keplerian rate. Thus the tangential component of the electric field in the system of coordinates rotating with the disk is zero,

$$[(\mathbf{v} - \mathbf{v}_d) \times \mathbf{B}]_{r,\phi} = 0, \quad (35)$$

at $z = 0$, where $\mathbf{v}_d = v_K \mathbf{e}_\phi$ and \mathbf{v} is the fluid velocity just above the disk. This condition means that in this system of coordinates rotating with the disk, the poloidal velocity is parallel to the poloidal magnetic field at $z = 0$.

The magnetic field is frozen into the disk so that $B_z = B_{dz}(r)$, where B_{dz} is a given function of r and is determined by the z -component of the initial monopole magnetic field. Notice that the two other field components, B_r and B_ϕ , are not fixed on the disk and change with time so as to satisfy the MHD equations in the computational region.

We suppose that the density and entropy on the disk surface are fixed, $\rho = \rho_d(r)$, $S = S_d(r)$, where $\rho_d(r)$ and $S_d(r)$ are given functions of r that follow from equations (29) and (31).

Note that in the present work the velocity of outflow from the disk is a free variable. This is different from our earlier work (Ustyugova et al. 1995). When the velocity of outflow from the disk is less than the slow magnetosonic speed, then the number of boundary conditions we have is sufficient. However, if the outflow velocity is superslow magnetosonic, then there should be an additional boundary condition. Because we do not have this additional bound-

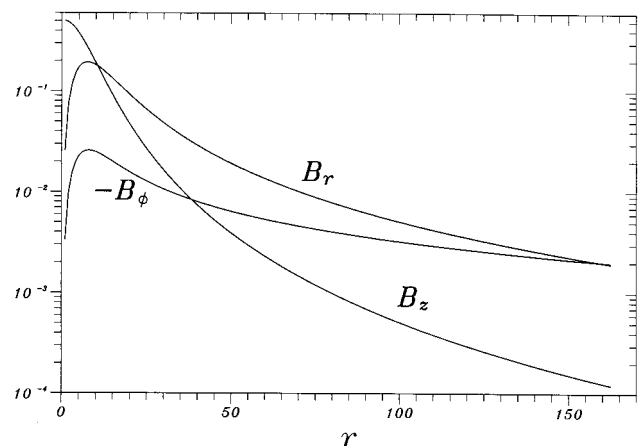


FIG. 4.—Radial dependences of the different components of the initial magnetic field on the surface of the disk.

ary condition, we suppose that the amplitudes of the corresponding outgoing waves are equal to zero. This is equivalent to the fact that we use the values of calculated parameters in the cells just above the disk.

On the z -axis, all fluxes normal to this axis are equal to zero. On the outer boundaries, $r = R_{\max}$ or $z = Z_{\max}$, the “free” boundary conditions $\partial F_j / \partial n = 0$ were used for all variables, excluding B_ϕ . Here $\partial / \partial n$ is the derivative perpendicular to the boundary, $F_j = \{\rho, f(S), v_r, v_\phi, v_z, B_r, B_z\}$. Our earlier simulation study (Romanova et al. 1997) showed that the condition $\partial B_\phi / \partial n = 0$ can lead to unphysical results. The outer boundary condition on B_ϕ is considered in detail in § 4.

4. INFLUENCE OF BOUNDARY CONDITIONS ON FLOW

If the process of outflow formation is strongly nonstationary, then the problem of the influence of outer boundary conditions may not appear. This is because it is difficult to separate the influence of boundary conditions from effects connected with nonstationarity. However, when the flow goes to a steady state, we observed that the stationary flow pattern can depend on the imposed outer boundary conditions and in some cases on the shape of the simulation region.

It is important to eliminate the influence of boundary conditions. It is possible, if (1) the flow is supersonic (superfast magnetosonic) and it is *perpendicular* to the outer boundaries (then information flows out of the simulation region), or (2) the correct boundary conditions are chosen by some method. The first condition cannot be realized during the stage of establishing of the flow, because initially the flow is subsonic. If the flow is supersonic but is not perpendicular to the boundary, then the Mach cones may be partially directed inside the simulation region and even supersonic flow may influence the flow inside the region. The orientation of the Mach cones depends in general on the shape of simulation region.

The second condition can be realized only in some approximation. The “best” outer boundary conditions are those which influence only the vicinity of the boundaries and not the central part of the simulation region. This involves all flow variables, but we will discuss only the outer boundary condition on B_ϕ , because we found that this condition had the strongest influence on the calculated flows.

The final flow may depend on both the Mach cone orientation at the boundaries (shape of the region) and on the outer boundary condition on B_ϕ . In different situations one of these factors may be more important than the other. To separate their influence on the final flow pattern, we discuss in § 4.1 simulations for a fixed simulation region but with different outer boundary conditions on B_ϕ . Next, in § 4.2 we fixed the boundary condition on B_ϕ and investigated the dependence of the flow on the shape of simulation region and the Mach cone orientation at the outer boundaries. In § 4.3 we discuss both factors.

4.1. Dependence of Flows on Outer Boundary Condition on B_ϕ

Here we present results of simulations for a fixed, elongated simulation region, $R_{\max} = 50r_i$, $Z_{\max} = 200r_i$, for three different outer boundary conditions on B_ϕ : (1) a standard “free” boundary condition, (2) a “force-free” boundary condition, and (3) a “force-balance” boundary condition.

4.1.1. “Free” Boundary Condition

Initially we performed simulations for the simplest standard “free” boundary condition on B_ϕ , $\partial B_\phi / \partial n = 0$. We observed that this boundary condition may give an artificial force on the boundary, which influences the flow within the computational region. For example, if we suppose that on the top boundary $\partial B_\phi / \partial z = 0$, then the radial component of the current density equals to zero, $j_r = -(c/4\pi)\partial B_\phi / \partial z = 0$, which means that the poloidal current density has only a z -component $\mathbf{j}_p = j_z \hat{z}$. This means that the poloidal current-density \mathbf{j}_p is not parallel to the poloidal magnetic field \mathbf{B}_p . Consequently, there is a force (density) $\mathbf{j}_p \times \mathbf{B}_p / c \neq 0$ acting in the ϕ direction, which is opposite to the rotation of the disk. Figure 5 shows the geometry.

These “boundary” forces act such way that the flow never reaches a stationary state. To check this fact and to be sure that this is not an effect of nonstationarity of our initial configuration, we did simulations for cases that went to a stationary state with other outer boundary conditions. After establishing stationarity, we substituted the outer boundary conditions on B_ϕ to a “free” boundary condition. We observed that the stationary state was destroyed for the reasons mentioned above. Figures 6a and 6b demonstrate one stage of this destruction, when the poloidal velocity decreased and became less than fast magnetosonic speed in all of the computational region. Even the fluxes of mass and other physical parameters through the boundaries are not constants in this simulation. Also, matter with magnetic flux enters the region from the right-hand side, which is due to the flow being subfast magnetosonic.

To avoid this artificial force, we proposed a “force-free” outer-boundary condition on B_ϕ (Romanova et al. 1997) that we discuss in the next subsection.

4.1.2. “Force-Free” Boundary Condition

Another possibility to consider is that the toroidal component of the magnetic force is zero on the outer boundaries. That is, $\mathbf{j}_p \parallel \mathbf{B}_p = 0$ on the outer boundaries. We can write this condition as

$$\mathbf{B}_p \cdot \nabla(rB_\phi) = 0. \quad (36)$$

We performed simulations with this boundary condition in the elongated region and observed that the flow reached a stationary state (see Figs. 6c and 6d). This flow has many characteristics of stationary flow. Fluxes of mass, energy,

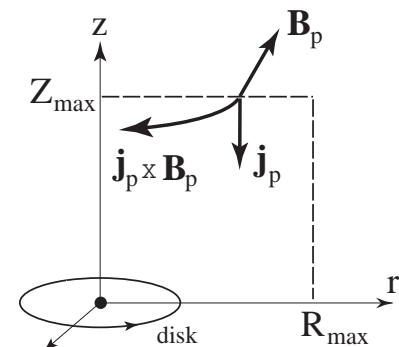


FIG. 5.—Artificial force $\mathbf{j}_p \times \mathbf{B}_p$ that can appear on the top outer boundary of the simulation region in the case of a “free” boundary condition on B_ϕ . Here \mathbf{B}_p and \mathbf{j}_p are the poloidal magnetic field and current density.

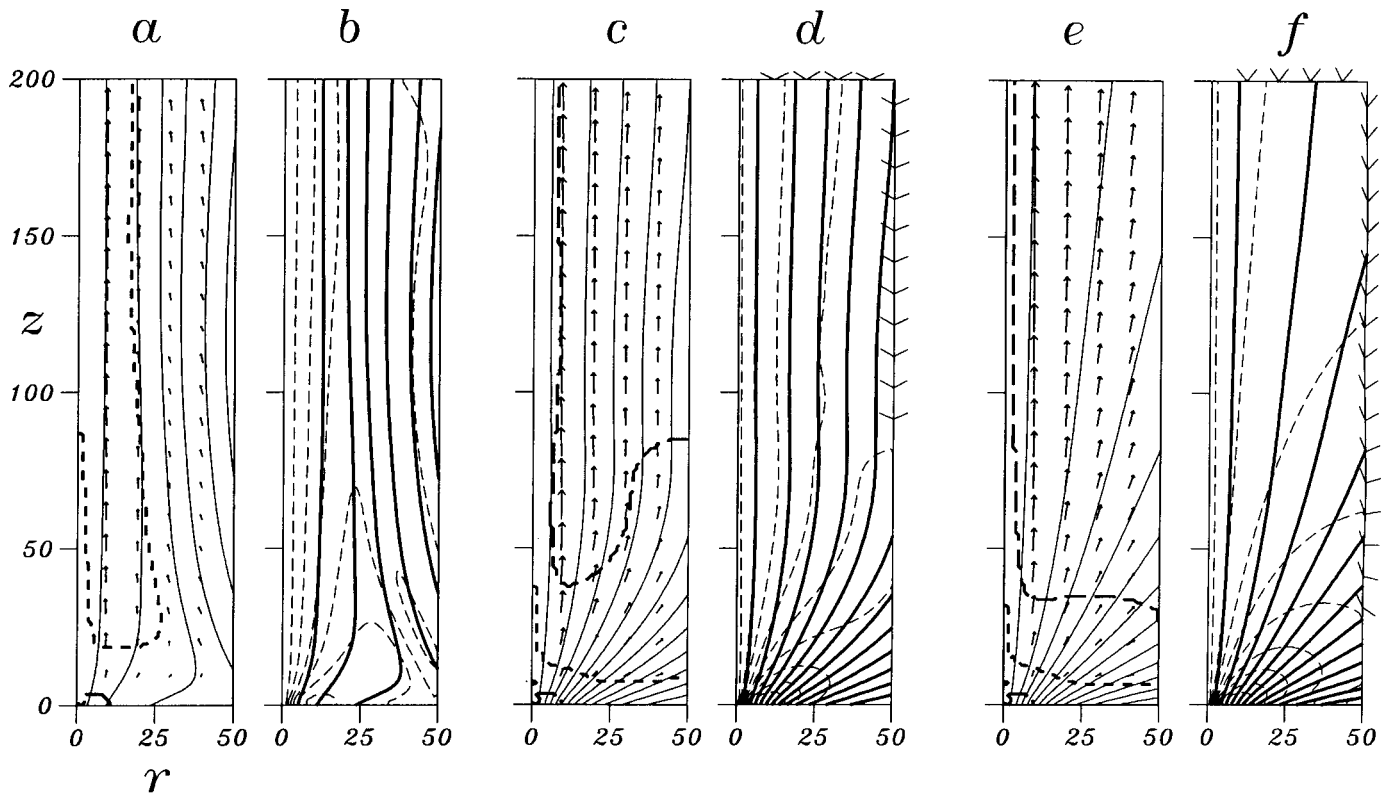


FIG. 6.—Results of simulations using a narrow computational region $R_{\max} = 50r_i$, $Z_{\max} = 200r_i$ for different outer boundary conditions on B_ϕ . Panels (a) and (b) correspond to a “free” boundary condition on B_ϕ , (c) and (d) to a “force-free” boundary condition, and (e) and (f) to a “modified” boundary condition. The solid lines represent the poloidal magnetic field or flux lines $\Psi = \text{constant}$ and the arrows the velocity vectors. The dashed lines in panels (b), (d), and (f) represent the level lines of the current density. The dashed lines in panels (a), (c), and (e) represent the slow magnetosonic (lowest dashed line), the Alfvén (middle dashed line), and the fast magnetosonic (furthest from the disk) surfaces. The Mach cones are shown at the boundaries of panels (d) and (f).

and momentum integrated over different cross sections are constants. Integrals of motion along magnetic field lines are also constants. The flow is *well collimated* inside the simulation region (see Figs. 6c and 6d). However, more detailed analysis (see § 4.2) shows that this collimation is artificial. The “force-free” boundary condition for B_ϕ is superior to the “free” boundary condition because it leads to a stationary state, but it does not give the physically correct flow. In reality, the magnetic force should not be zero on the boundary. There is a magnetic force pushing matter outward through the outer boundaries. One can see from Figure 6d that the poloidal current density (dashed lines) is not parallel to the poloidal magnetic field (solid lines). However, on the boundaries (Fig. 6d) the two vectors are forced to be parallel, and thus the poloidal force equals zero. This boundary condition is better than the “free” boundary condition in the sense that there is no strong artificial force at the boundary. From the other side, when we put the force equal to zero, it is analogous to application of a force equal to the real force but with the opposite sign.

This is one of the factors that may lead to artificial collimation. Another possible factor (Mach-cone orientation) depends on the shape of the simulation region and is discussed in § 4.2.

4.1.3. “Force-Balance” Boundary Condition

As a next step for improving the outer boundary condition on B_ϕ , we take into account the fact that the magnetic field is not force-free, and \mathbf{j}_p is not parallel to \mathbf{B}_p . We start

from equation (16) for B_ϕ and write it in the form

$$rB_\phi = \Omega \sqrt{4\pi\rho_A} \frac{r^2 - r_A^2}{1 - \rho_A/\rho} \approx -\Omega \sqrt{\frac{4\pi}{\rho_A}} \rho r^2, \quad (37)$$

where we assume that the density at the boundary is much less than that at the Alfvén surface, $\rho \ll \rho_A$ for $r^2 \gg r_A^2$. Then we obtain

$$\begin{aligned} \mathbf{B}_p \cdot \nabla(rB_\phi) &= -\Omega \sqrt{\frac{4\pi}{\rho_A}} \mathbf{B}_p \cdot \nabla(\rho r^2) \\ &= rB_\phi (\mathbf{B}_p \cdot \nabla) \ln(\rho r^2) = \alpha B_r B_\phi, \end{aligned} \quad (38)$$

where we supposed that $\rho r^2 = F(\Psi)r^2$ and took into account that Ω and ρ_A are constants along magnetic field lines.

Finally, we obtain the outer-boundary condition as

$$\mathbf{B}_p \cdot \nabla(rB_\phi) = \alpha B_r B_\phi, \quad (39)$$

where α is a parameter. In this case we got stationary flows that are *not collimated* in the simulation region (see Figs. 6e and 6f). Fluxes through the outer surfaces and integrals along magnetic field lines are well conserved, as in the case of collimated flow, described in § 4.1.2.

The question arises: which boundary condition is correct, “force-free” or “force-balance”? The “force-balance” condition is clearly the physical condition, because it does not generate an artificial force on the boundary. However, it is more difficult to apply, because there is no direct method

for determining the parameter α . It can only be obtained iteratively using additional simulations, which is very time consuming. Our analysis indicates that the “force-free” boundary condition gives good results as compared with those obtained using the “force-balance” condition if the shape of the simulation region is not elongated in the z -direction.

Below, we investigate different runs for “force-free” outer boundary conditions on B_ϕ but for different shapes of the simulation region.

4.2. Dependence of Flows on Shape of Region: Orientation of Mach Cones

We noticed empirically that results of simulations depend significantly on the shape of simulation region. The ratio between R_{\max} and Z_{\max} is critical. We observed that when the region is elongated in z -direction, then the flow has tendency to collimate. When the region is square, spherical, or elongated in r -direction, then the outflow is almost spherical, that is, only slightly collimated. Here we present results of simulations all with “force-free” outer boundary conditions but different shapes of the simulation region.

We first investigated the case where the height of the region is the same as before, $Z_{\max} = 200r_i$, but the region is much wider, $R_{\max} = 170r_i$. Figure 7 shows that in this case we got almost spherical outflow, which is very different from the well-collimated outflow in the narrow region at the same boundary conditions (Figs. 6c and 6d). We also performed similar simulations in spherical coordinates with $R_{\max} = 170r_i$ and got similar results. The question is why the flows are so different for different shapes of the simula-

tion region. In all cases the flow is superfast magnetosonic in most of the region. However, note that even if the flow is superfast magnetosonic, information can flow in from the boundaries to the simulation region if the Mach cones are directed inside the simulation region.

The Mach cone projected onto the poloidal plane has a half opening angle φ , which is

$$\tan^2 \varphi = \frac{(v_A^2 + c_s^2)(v_p^2 - v_c^2)}{(v_p^2 - c_{sm}^2)(v_p^2 - c_{fm}^2)}, \quad (40)$$

where c_{sm} and c_{fm} are the slow and fast magnetosonic velocities, respectively, which satisfy $c_{s, fm}^4 - c_{s, fm}^2(c_s^2 + v_A^2) + c_s^2 v_{Ap}^2 = 0$ [with $v_A^2 = B^2/(4\pi\rho)$ and $v_{Ap}^2 = B_p^2/(4\pi\rho)$], and $v_c \equiv v_{Ap} c_s / (v_A^2 + c_s^2)^{1/2}$ is the “cusp” velocity (Polovin & Demutskii 1980; Lovelace et al. 1986; Bogovalov 1997). Figures 6–8 show the Mach cones on the outer boundaries for different shapes of the simulation region. We find that in the case of an elongated region (Fig. 6d), an essential part of the Mach cones is directed into the simulation region, whereas in the case of an almost square region (Fig. 7b), only very small part of the Mach cones is directed into the region. Figure 8 shows that the most desirable geometry—where information flows outward across the outer boundary—is obtained in spherical coordinates where all Mach cones are directed outward from the simulation region. The elongated region is the least desirable and, as is discussed, gives artificial collimation of the flow. Note that the first stationary MHD flow solutions (Romanova et al. 1997) were obtained using a simulation region elongated in the r -direction.

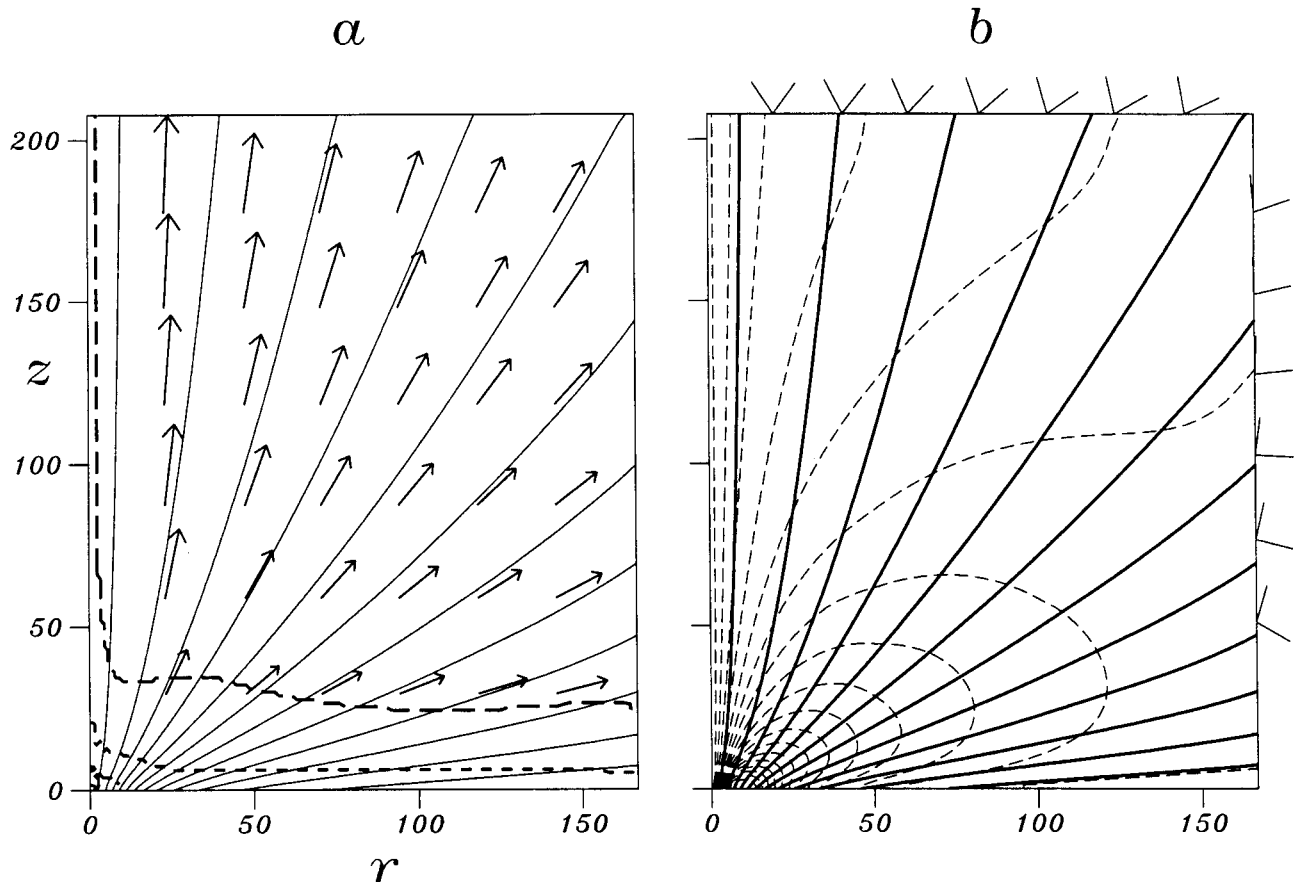


FIG. 7.—Results of simulations for an approximately square simulation region $R_{\max} = 170r_i$, $Z_{\max} = 200r_i$ using the “force-free” outer boundary condition on B_ϕ . Here r and z are measured in units of r_i , which is the inner radius of the disk. The lines and arrows have the same meaning as in Fig. 6.

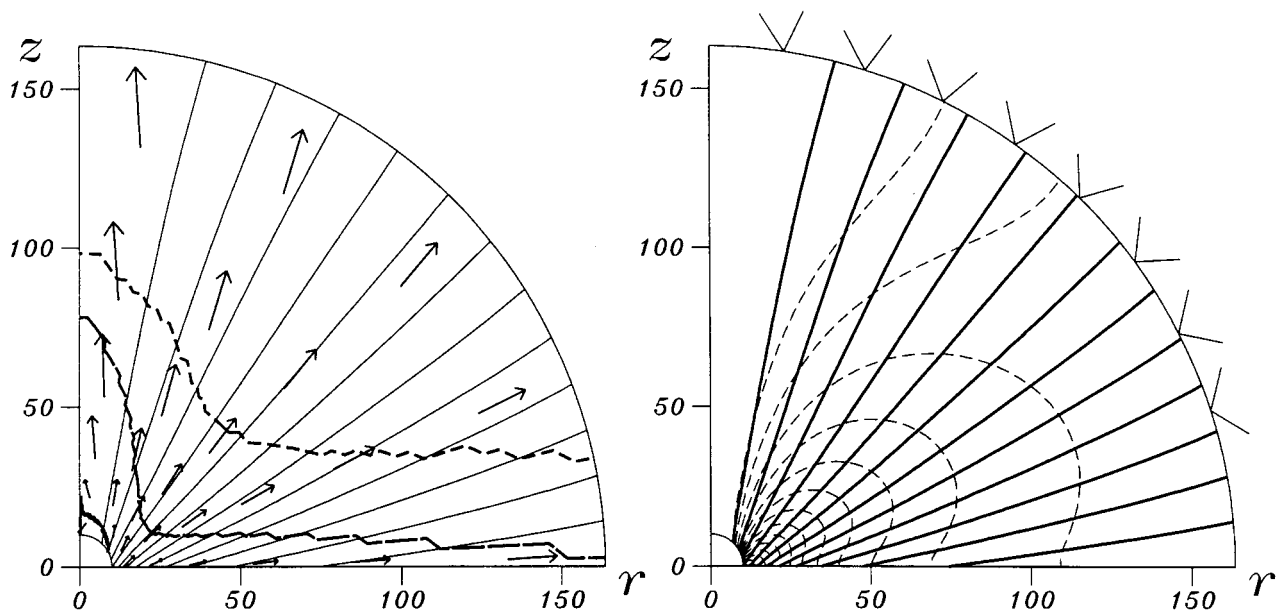


FIG. 8.—Results of simulations for the same case as Fig. 7 but using a spherical coordinate system and simulation region

4.3. Discussion of Boundaries

Regarding the outer boundaries, we conclude that simulated flows may depend on both the outer boundary condition on B_ϕ and the shape of simulation region (the Mach cones' orientation on the outer boundary). The influence of each of these factors may be different in different situations.

The orientation of the Mach cones at the boundary is not connected directly with existence and configuration of a stationary flow. However, if Mach cones are partly directed inside the simulation region along part of the outer boundary, then the question arises: what is the result of this influence, and how strong is it? Our simulations show that for a "force-free" boundary condition on B_ϕ the result is artificial collimation of the flow, whereas in the case of a "free" boundary condition, there is destruction of a stationary flow that was arranged as an initial condition.

From comparison of cases shown in Figures 6d and 7b it is not clear that Mach cones are responsible for the collimation of the flow in the case shown in Figure 6d. In the narrow region the magnetic field at the right-hand, outer boundary is much stronger than in the case of wide region, so influence of the nonexact "force-free" boundary condition should be stronger in the case of a narrow region. To check this possibility, we performed simulations in a small square region with $R_{\max} = 50r_i$ and $Z_{\max} = 50r_i$ and found uncollimated, almost spherical outflow. This indicates that the shape of the region is the most important factor affecting collimation.

Another question is evident. Why in the case of the "force-balance" boundary condition on B_ϕ in the elongated region do we find the physically correct stationary solution? We suggest that during establishment of the stationary flow, which may be quite violent (in spite of almost stationary initial conditions), this boundary condition kept the approach to stationarity less violent (than in the case of "force-free" boundary conditions) and the Mach cones directed outward most of the time. The fact that in this case a small part of the Mach cones is directed inside the region means that some inflow of information from the outer boundary may have only a small affect on the flow.

For some purposes, such as the study of the propagation of jets, it is attractive to use a long, narrow computational region. The general conclusion of this section is that a narrow region can lead to artificial collimation of the flow or invalid solutions unless special care is given to the boundary condition on B_ϕ .

5. STATIONARY FLOWS: COMPARISONS OF SIMULATIONS WITH THEORY

Here we describe results of simulations for a region $R_{\max} = 170r_i$ and $Z_{\max} = 200r_i$ with a "force-free" outer boundary condition. Simulations of the flow in the same region but with the "modified" boundary condition gave similar results.

Figure 9 shows the initial distribution on the disk of the Keplerian velocity v_K , the poloidal Alfvén velocity v_{Ap} , and the sound speed c_s . Matter outflowing from the disk has a

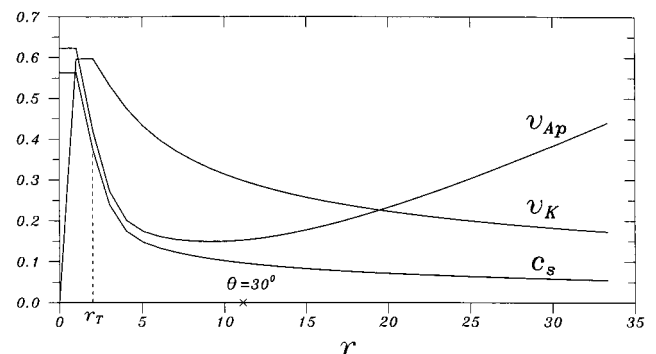


FIG. 9.—Dependences of velocities on r (in units of r_i) along the disk in the stationary state, where r_i is the inner radius of the disk. Here v_K is the Keplerian velocity, c_s the sound speed, and v_{Ap} the poloidal Alfvén velocity, measured in units of $v_i \equiv \sqrt{GM/r_i}$. The point $\theta = 30^\circ$ shows the location on the disk where the poloidal magnetic field is inclined to the z -axis at an angle $\theta = 30^\circ$; for larger r we have $\theta > 30^\circ$. We show only $r \leq 35r_i$, because the magnetic field lines that start at larger r are highly inclined away from the z -axis and also do not pass through the fast magnetosonic surface within our simulation region (see Fig. 7). Inside the radius r_T the disk is relatively hot (see eq. [29]).

time-independent distribution of density as a function of radius. The velocity of outflow from the disk is determined by the solution of the MHD equations in the simulation region. The simulations show that in a stationary state, matter just above the disk has a velocity somewhat larger than the slow magnetosonic velocity. This is in accord with the theory, which indicates that the slow magnetosonic surface is located inside the disk (Lovelace, Romanova, & Contopoulos 1993).

Moving away from the disk, matter starts from a low velocity, is gradually accelerated, and crosses the Alfvén and fast magnetosonic surfaces (see Fig. 7a). These surfaces are almost parallel to the disk. Figure 10a shows the variation of different velocities along a representative magnetic field line, the third line away from the z -axis in Figure 7, on the flow distance s from the disk. This field line, which we refer to as the “reference” field line, crosses the top boundary at about the midpoint of this boundary. This line is not special, but it is inclined sufficiently to the axis that magnetic/centrifugal forces are important. Figure 10a shows in particular the dependence of the poloidal velocity $v_p(s)$, which becomes larger than the Alfvén velocity v_{Ap}

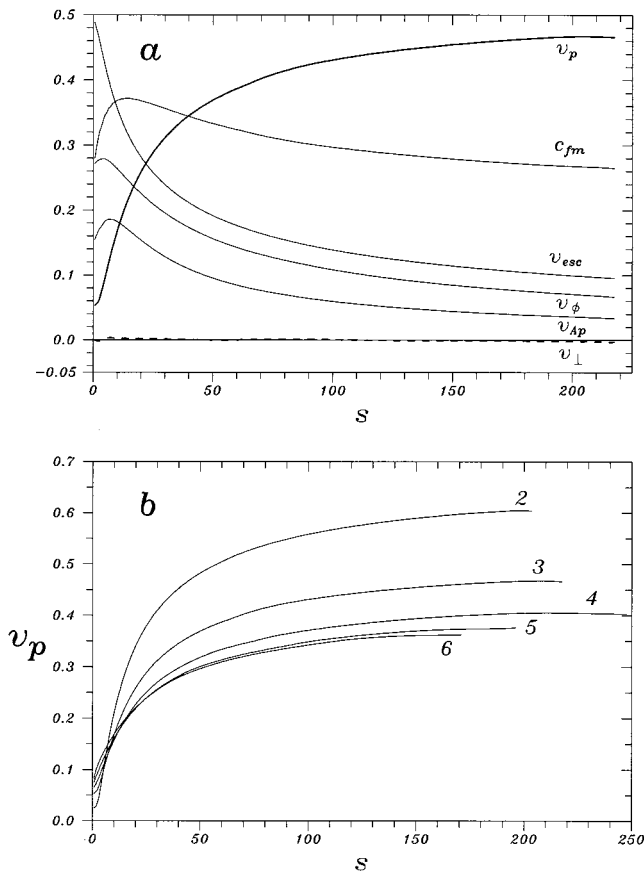


FIG. 10.—Panel (a) shows the dependences of different velocities on distance s measured in units of r_i from the disk along the “reference” magnetic field line. The velocities are measured in units of $\sqrt{GM/r_i}$. The “reference” field line is the third field line away from the z -axis in Fig. 7a. This field line crosses the top boundary about in the middle. This field line “starts” from the disk at $r \approx 6r_i$, where it has an angle $\theta \approx 28^\circ$ relative to the z -axis. Here v_p is the poloidal velocity along the field line, and v_\perp is the poloidal velocity perpendicular to the field line. Also, v_{Ap} is the poloidal Alfvén velocity, c_{fm} is the fast magnetosonic velocity, and v_{esc} is the local escape velocity. Panel (b) shows the dependences of $v_p(s)$ for different field lines identified by the number of the field line counted away from the z -axis in Fig. 7a.

fairly close to the disk, at $s > 10r_i$. Furthermore, v_p becomes larger than the local escape velocity v_{esc} for $s > 25r_i$. At larger distances, v_p becomes larger than the fast magnetosonic velocity c_{fm} at $s > 40r_i$, and it approaches an asymptotic speed that is about 1.75 times c_{fm} at the outer boundary of the simulation region. The poloidal velocity is parallel to the poloidal magnetic field to a good approximation, which is in accord with the theory. Figure 10b shows the dependences of $v_p(s)$ for different field lines.

Within the simulation region, the outflow accelerates from thermal velocity to a much larger asymptotic poloidal flow velocity of the order of $0.5\sqrt{GM/r_i}$. Thus the *acceleration distance* for the outflow, over which the flow accelerates from $\sim 0\%$ to, say, 90% of the asymptotic speed, occurs at a flow distance of about $80r_i$.

5.1. Mechanism of Acceleration

Figure 11 shows the different forces acting along the “reference” magnetic field line. The centrifugal force (C) is larger than the magnetic (M) or pressure gradient force (P) immediately above the disk $s < 10r_i$. The magnetic force is a few times larger than the centrifugal force for larger distances, $s > 10r_i$. Note that the pressure gradient force is negligibly small. Thus the main driving forces pushing matter outward are magnetic and centrifugal.

Each poloidal magnetic field line is labeled by its Ψ value, which is proportional to the magnetic flux through the circular region between the axis and the field line. Ψ increases from zero on the axis to a largest value on the field line most distant from the axis. We integrated the forces to obtain the total work performed by the magnetic, centrifugal, and other forces along different field lines from the disk to the outer boundary. Figure 12 shows the dependence of this work on Ψ . One can see that near the axis (small Ψ) the main work is performed by the centrifugal force, while the magnetic force is also important. The work along the “reference” field line, marked by “ r ” on the Ψ axis, is done mainly by the magnetic force with the centrifugal force also important. Going away from the axis to larger Ψ and more inclined magnetic field lines, one can see that the magnetic force is more and more important. Note that the work done by the pressure gradient is small for all field lines.

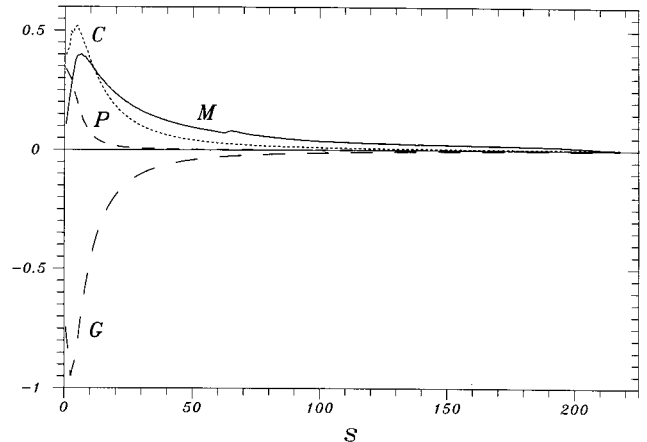


FIG. 11.—Forces acting along the “reference” field line. M is the magnetic force, C the centrifugal force, P the pressure gradient force, and G the gravitational force. The distance s is measured in units of r_i . The scale for forces is arbitrary.

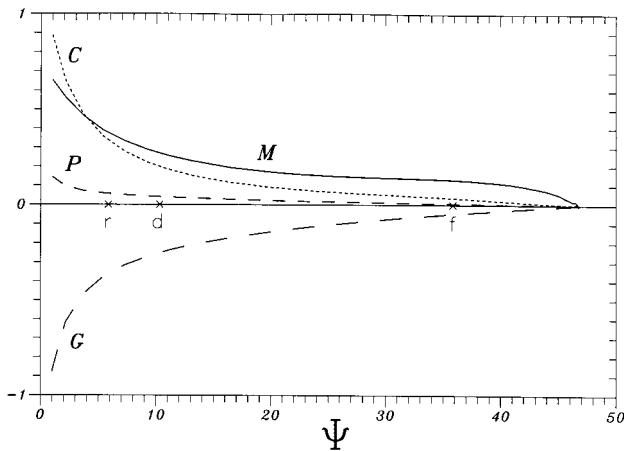


FIG. 12.—Work done by the different forces along different field lines from the disk to the outer boundary. Each field line is labeled by its value of Ψ . The field line corresponding to our “reference” line is marked “ r ,” and the “diagonal” field line that goes through the top right corner of the simulation region is marked “ d .” The point “ f ” is the largest radius at which the flow goes through the fast magnetosonic surface. The letters M , C , P , and G stand for magnetic, centrifugal, pressure gradient, and gravity forces.

5.2. Analysis of Stationarity

A first indication of stationarity is when the fluxes of mass and other physical quantities become constants in time. We observed that the fluxes of mass \mathcal{F}_M , angular momentum \mathcal{F}_L , and energy \mathcal{F}_E calculated through the middle of the region $z = 0.5Z_{\max}$ become constants after about $t > 200t_i$, where $t_i \equiv 2\pi r_i/v_i$, where $v_i \equiv \sqrt{GM/r_i}$ and r_i is the inner radius of the disk. The time dependence of the fluxes is shown in Figure 13. We performed simulations for much longer times, $t \sim 3500t_i$, and observed that these fluxes were accurately constants in time. Note that this time corresponds to only $t = 1.6t_{\text{out}}$, where $t_{\text{out}} = t_i(r_{\text{out}}/r_i)^{3/2} = 2216t_i$. This indication of stationarity is necessary but not a sufficient sign of a valid stationary MHD flow.

Another indication of stationarity is that the poloidal velocity becomes parallel to the poloidal magnetic field. We observed that the two vector fields become parallel to a high accuracy only after $t > t_{\text{out}}$. Figure 7a shows that the two vector fields are close to being parallel even at earlier times.

One can get more complete information about stationarity and validity of the MHD flow by comparing the theory reviewed in § 3 with the simulation data. First, the

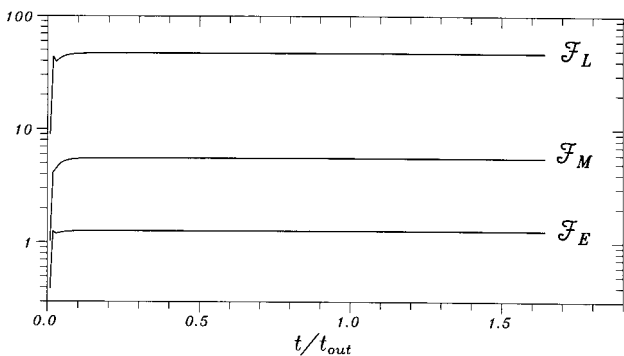


FIG. 13.—Fluxes of mass \mathcal{F}_M , angular momentum \mathcal{F}_L , and energy \mathcal{F}_E across the area $z = 0.5Z_{\max}$ as a function of time. Time is measured in units of $t_{\text{out}} \approx 2200t_i$, where $t_i \equiv 2\pi r_i/\sqrt{GM/r_i}$ and r_i is the inner radius of the disk.

integrals of the motion, Λ , K , E , Ω , and S (eqs. [4]–[8]) should be constants along any magnetic field line. We checked this by numerically calculating these integrals along the “reference” magnetic field line. The calculated integrals are constants with good accuracy. For example, $|\Delta\Omega|/\Omega \lesssim 0.06$ and $|\Delta S|/S \lesssim 0.15$. Figure 14 shows variation of the integrals. Note that the integrals are not strictly constants in the region immediately above the disk because the grid is not fine enough in this region because of the strong gravitational force. Note that the integrals become constants as a function of Ψ much later ($t \gtrsim t_{\text{out}}$) than fluxes of mass, angular momentum, and energy become constants in time.

Other comparisons of simulations with theory have been done. For example, from the theory of stationary flow it follows that fluxes of matter, angular momentum, and energy flowing inside a given flux tube should be equal to fluxes integrated over the Alfvén surface, equations (17)–(19). We calculated these integrals in two ways, using the data from our simulations. Figures 15a and 15b show these integrals as a function of Ψ . They almost coincide in most of the region, excluding the region of large values of Ψ . The latter field lines have a high angle of inclination relative to the axis and do not pass through the fast magnetosonic surface. These lines are marked by the long-dashed lines on one of the curves and by the letter f on the Ψ axis.

Figure 16 shows the Ψ dependence of the ratio of the radii where a magnetic field line crosses the Alfvén surface and the disk, $\lambda = r_A(\Psi)/r_d(\Psi)$. This ratio is of interest, because the value of the angular momentum per unit mass carried by the outflowing matter can be calculated as

$$\Lambda = \Omega r_A^2 = \lambda^2 [GM r_d(\Psi)]^{1/2} \quad (41)$$

from equation (14). The fact that λ is almost constant means that the specific angular momentum is proportional to $\sqrt{r_d}$ and can be estimated in this way. Specifically, $\Delta\lambda/\lambda \lesssim 0.13$ for field lines that cross the fast magnetosonic surface.

The fluxes of mass, energy, and angular momentum flowing out from the disk depend of course on the magnetic field strength on the disk. Figure 17 shows the dependence of the matter outflow rate on the disk magnetic field. This dependence is analogous to that derived by Kudoh &

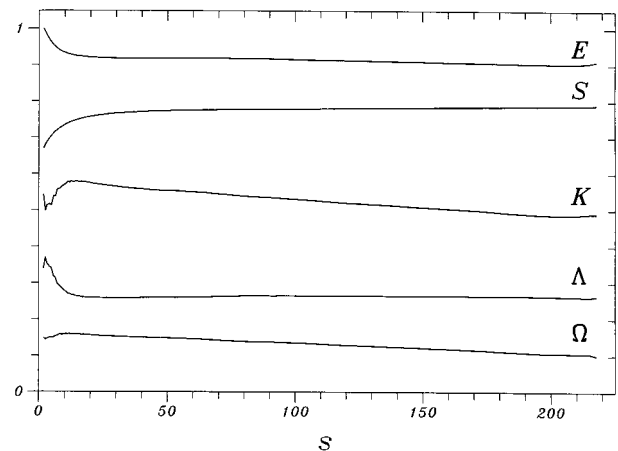


FIG. 14.—Numerically calculated “integrals of the motion” (eqs. [1]–[5]) as a function of distance s along the “reference” magnetic field line. In ideal MHD, the integrals should be strictly constant. In this plot the scale is such that the maximum of the E integral is unity. The other curves have been displaced downward for clarity.

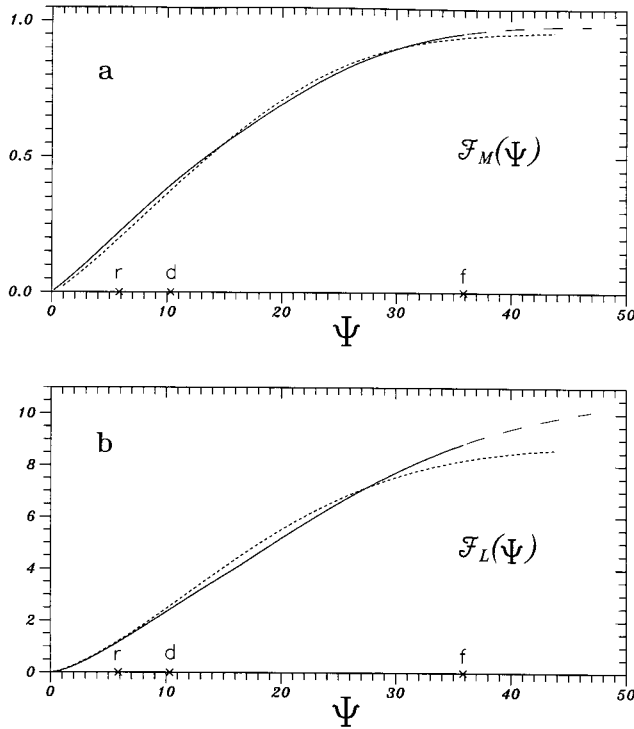


FIG. 15.—Panel (a) shows the matter flux and panel (b) the angular momentum flux as a function of Ψ calculated in two ways. The solid line shows the integrals calculated using eqs. (11) and (12). The dashed line shows the integrals calculated on the Alfvén surface using eqs. (17) and (18). Points r , d , and f on the horizontal axis are the same as in Fig. 12. The long-dashed line shows the region of strongly inclined field lines that do not cross the fast magnetosonic surface. These field lines are separated from the other field lines by f on the Ψ axis.

Shibata (1995, Fig 2b; 1997b, Fig 24b), who performed a 1.5 D analysis of stationary MHD flows at the fixed configuration of poloidal magnetic field.

5.3. Collimation

The stationary MHD outflows we find are approximately spherical outflows with relatively small collimation within the simulation region. Thus the collimation distance over which the flow becomes collimated (with divergence less than, say, 10°) is much larger than the size of our simulation region. Figure 18 shows the dependence of the angle between the poloidal field direction and the z -axis on the distance along the “reference” magnetic field line (θ_1) and along the “diagonal” field line that goes through the top right corner of the simulation region (θ_2). Both angles are

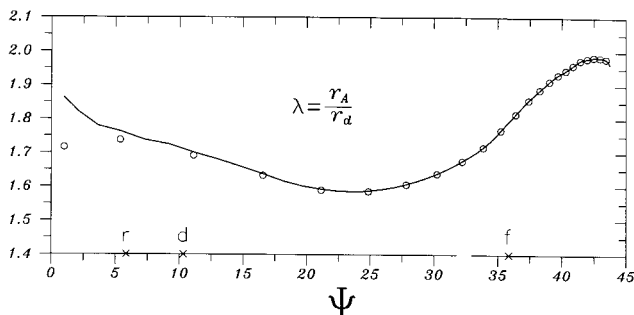


FIG. 16.—Ratio $\lambda = r_A(\Psi)/r_d(\Psi)$ as a function of Ψ . Points r , d , and f are the same as in Fig. 12.

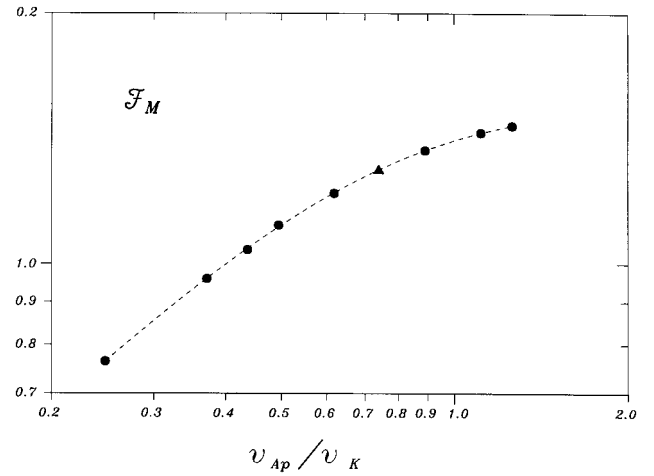


FIG. 17.—Dependence of matter flux from the disk on the ratio v_{Ap}/v_i evaluated at the inner radius of the disk, $r = r_i$. Here we changed only the magnitude of the magnetic field B_p , while all other parameters were kept the same. The triangle indicates the main case of the paper, while the circles were obtained from different runs. The dashed line is simply a curve through the points.

relatively large (greater than 30°) near the disk and then gradually decrease at larger distances s along the field line. This means that some collimation occurs near the disk but decreases at larger distances. The angle θ_1 for the “reference” field line changes from 35° at the disk to 18° at the top boundary, where the angle of the position vector from the origin to the z -axis is about 20.5° . The angle θ_2 for the “diagonal” field changes from 49° at the disk to 31° at the top boundary, where the angle of the position vector from the origin to the z -axis is about 39° .

An important question is whether the outflow becomes collimated at large distances to form a cylindrical jet parallel to the rotation axis or continues as a wind without collimation. To obtain information on this question, we calculated the derivatives $\partial\theta/\partial s$ along magnetic field lines as also shown in Figure 18. For both the “reference” and the diagonal field lines the derivatives decrease and become very small at the outer boundary. It appears that the derivatives continue to decrease, which would mean that the collimation decreases and goes to zero. (The turns at the

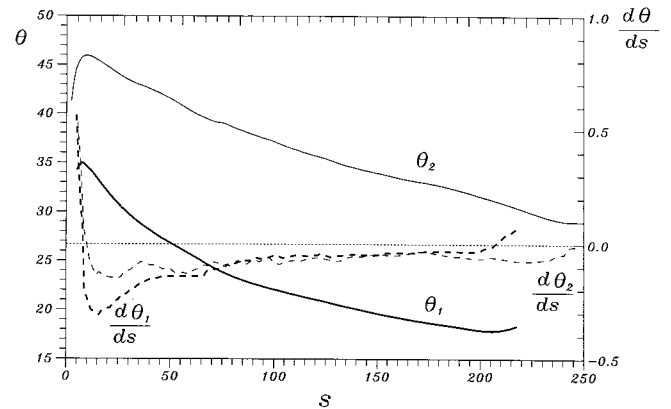


FIG. 18.—Dependence of the angle θ between the poloidal magnetic field and the z -axis as a function of distance s along the field line. The dependence of the derivatives $\partial\theta/\partial s$ is also shown. The label “1” indicates our “reference” magnetic field line and “2” the “diagonal” field line discussed in the text.

ends of the lines are connected with boundaries and do not represent a real collimation effect.) However, the present study does not rule out the possible magnetic collimation of the flow at much larger distances. Separate simulations in a much larger region are needed to answer this important question.

Earlier, Sakurai (1987) obtained stationary flow solutions for a split-monopole magnetic field and found flows with very gradual collimation at large distances from the origin. Our results are similar in this respect to those of Sakurai. However, it is not clear that the flows will magnetically collimate to cylinders, as was predicted by Heyvaerts & Norman (1989). Simulations on a much larger region are needed to answer this question.

It is important to note that analytic, self-similar solutions for outflows for cases of very gradually decreasing poloidal magnetic field in the disk (unlike the present split-monopole field) show magnetic collimation with increasing distance z from the origin (Contopoulos & Lovelace 1994; Contopoulos 1995; Ostriker 1997). Furthermore, note that outflows may be collimated hydrodynamically by the pressure of surrounding ambient matter (Lovelace, Berk, & Contopoulos 1991; Frank & Mellema 1996; Mellema & Frank 1998).

It is of interest to compare the present results on collimation with those of our earlier studies, Ustyugova et al. (1995) and Romanova et al. (1997). Ustyugova et al. (1995) introduced the treatment of the disk as a boundary condition and found nonstationary but well-collimated outflows. Ustyugova et al. considered outflows from a hot accretion disk, where the sound speed $c_s \lesssim v_K$ and a weak magnetic field $v_A^2 \ll v_K^2$ on the disk surface. For such conditions, the main force driving the outflow is the matter pressure gradient, while the magnetic force is smaller. Also, Ustyugova et al. (1995) used nonequilibrium initial conditions, where the rotation of the disk was started at $t = 0$ with the corona of the disk not rotating. These conditions led to the formation of a strong toroidal magnetic field (by the winding up of the poloidal field) and a strong, outward-propagating torsional Alfvén wave. The fact that the Alfvén velocity was much smaller than the Keplerian velocity allowed the build up of the toroidal field, which in turn gave strong collimation of the outflow. At later times in the simulation the twist of the field relaxed, but the matter pressure force continued to push matter along the collimated magnetic field lines. Thus the Ustyugova et al. (1995) flows are essentially different from the stationary flows discussed in this paper, where the dominant driving forces are magnetic and centrifugal, with the matter pressure force being negligible.

Romanova et al. (1997) was the first simulation study to obtain *stationary*, magnetocentrifugally driven outflows with a relatively small matter pressure force. The initial poloidal magnetic field was a “tapered” monopole configuration. The outflows were found to be uncollimated and are therefore similar to those discussed in this paper for the split-monopole initial field.

5.4. Illustrative Physical Values

Here we discuss physical values of parameters for the case of MHD outflows from the disk around a young star. The mass of the star is considered to be $M = M_\odot \approx 2 \times 10^{33}$ gm, and the inner radius of the disk is $r_i = 10^{11}$ cm, which may be somewhat larger than the star’s radius. The magnetic field threading the accretion disk may arise from the

“shearing off” and opening of the intrinsic stellar field, as was discussed by Lovelace, Romanova, & Bisnovaty-Kogan (1995). The reference field strength at the inner edge of the disk is taken to be $B_i \equiv |\mathbf{B}_p(r_i, 0)| = 300$ G. The computational region extends from $(r, z) = 0$ to $(R_{\max}, Z_{\max}) = (170r_i, 200r_i)$, so that $R_{\max} = 1.7 \times 10^{13}$ cm. The characteristic velocity at the inner edge of the disk is $v_i \equiv (GM/r_i)^{1/2} \approx 365$ km s⁻¹. With our smoothed potential, the Keplerian velocity of the disk at r_i is $v_i/2^{3/4} \approx 0.6v_i$. The characteristic time at the inner edge of the disk is $t_i = 2\pi r_i/v_i \approx 4.8$ hr. The density on the surface of the disk at $r = r_i$ can be written in terms of the Alfvén velocity as $\rho_i = B_i^2/(4\pi v_{Ap}^2) \approx 6.8 \times 10^{-12}(v_i/v_{Ap})^2$ g cm⁻³.

We find that the mass outflow rate from the top side of the disk has the dependence

$$\begin{aligned} \dot{M}_+ &= \mathcal{F}_M r_i^2 B_i^2 / v_{Ki} \\ &\approx 4 \times 10^{-7} \frac{M_\odot}{\text{yr}} \mathcal{F}_M \left(\frac{r_i}{10^{11} \text{ cm}} \right)^{5/2} \left(\frac{B_i}{300 \text{ G}} \right)^2 \left(\frac{M_\odot}{M} \right)^{1/2}, \end{aligned} \quad (42)$$

where $\mathcal{F}_M = \mathcal{F}_M(v_A/v_i)$ (see Figure 17). For the reference case (§ 5), $\mathcal{F}_M \approx 5.6$ so that $\dot{M}_+ \approx 2.2 \times 10^{-6} M_\odot \text{ yr}^{-1}$. The total mass outflow from the disk is evidently $2\dot{M}_+$.

Similarly, we can write the energy outflow rate from the top of the disk as

$$\begin{aligned} \dot{E}_+ &= \mathcal{F}_E r_i^2 B_i^2 v_{Ki} \\ &\approx 1.5 \times 10^{34} \frac{\text{ergs}}{\text{s}} \mathcal{F}_E \left(\frac{r_i}{10^{11} \text{ cm}} \right)^{3/2} \left(\frac{B_i}{300 \text{ G}} \right)^2 \left(\frac{M}{M_\odot} \right)^{1/2}. \end{aligned} \quad (43)$$

For our reference case (§ 5) $\mathcal{F}_E \approx 1.2$ so that $\dot{E}_+ \approx 2.5 \times 10^{35}$ ergs s⁻¹. The total energy outflow from the disk is $2\dot{E}_+$.

Matter is accelerated from $v_p \approx 0.05v_i \approx 18$ km s⁻¹ near the surface of the disk to $v_p \approx 0.47v_i = 170$ km s⁻¹ at the outer boundary of the simulation region (see Fig. 10).

6. CONCLUSIONS

We have studied MHD outflows from a rotating, conducting accretion disk using axisymmetric simulations. The disk was treated as a boundary condition, and the initial poloidal magnetic field was taken to be a split monopole. The main conclusions of this work are:

1. In many different runs we observed the formation of stationary MHD outflows from the disk. Close to the disk the main driving force is the centrifugal force. At larger distances the main driving force is the magnetic force $\propto -\nabla(rB_p)^2$. The pressure gradient force is much smaller than these forces, and it has no significant role in driving the outflows.

2. For the considered conditions, the slow magnetosonic surface lies inside the disk. Above the disk the flow accelerates and passes through the Alfvén and fast magnetosonic surfaces, which are almost parallel to the disk. Within the simulation region, the outflow accelerates from thermal velocity ($\sim c_s$) to a much larger asymptotic, poloidal flow velocity of the order of $0.5\sqrt{GM/r_i}$, where M is the mass of the central object and r_i is the inner radius of the disk. This asymptotic velocity is much larger than the local escape speed and is larger than fast magnetosonic speed by a factor

of ~ 1.75 . The *acceleration distance* for the outflow, over which the flow accelerates from $\sim 0\%$ to, say, 90% of the asymptotic speed, occurs at a flow distance $\sim 80r_i$.

3. The outflow is only slightly collimated within the simulation region. The *collimation distance* for the outflow, over which the flow becomes collimated (with divergence less than, say, 10°) is much larger than the size of our simulation region. This “poor” collimation is similar to that found in our earlier work (Romanova et al. 1997) using a different initial magnetic field and is qualitatively similar to the very gradual collimation found by Sakurai (1987). MHD simulations using much larger computational regions are needed to determine the collimation of the outflow at large distances. Furthermore, separate simulations are also needed to study the collimating influence of an external medium (Lovelace et al. 1991; Mellema & Frank 1998).

4. The stationarity of the MHD flows was checked in a number of ways, including comparisons of simulation results with predictions of theory of stationary axisymmetric flows. We found that: (1) fluxes of mass, angular momentum, and energy across the surface $z = 0.5Z_{\max}$ become independent of time with high precision at early times of simulations $t < 0.1t_{\text{out}}$, where $t_{\text{out}} \approx 2200t_i$ and $t_i = 2\pi r_i / \sqrt{GM/r_i}$; (2) integrals of the motion become constants on flux surfaces with accuracy $5\%–15\%$ for $t \gtrsim t_{\text{out}}$; and (3) vectors of poloidal velocity are parallel to those of the poloidal magnetic field lines to a high accuracy.

5. Different outer boundary conditions on the toroidal magnetic field B_ϕ were investigated. We analyzed simula-

tion results and found that the collimation of the jet and other characteristics of the flow depend critically on the outer boundary condition on B_ϕ (as well as the shape of the simulation region, as is discussed below). We observed that the outer, “free” boundary condition on B_ϕ leads to an artificial force that can give *apparent* magnetic collimation of the flow. “Force-free” and “force-balance” outer boundary conditions were also investigated. The “force-free” outer boundary condition was found to give valid flow solutions if the simulation region is not narrow in r -direction (compared with z -direction).

6. The question of the optimum shape of simulation region was investigated. We have shown that if region is narrow in the r -direction, then an essential part of the Mach cones on the outer boundaries may be directed toward the inside of the computational region. This can lead to the influence of the boundary on the calculated flow and to artificial collimation. This effect is reduced or absent if the computational region is approximately square, if it is elongated in the r -direction, or if it is spherical. In these cases the Mach cones tend to point outside of the computational region.

This work was supported in part by NSF grant AST 93-20068. The Russian authors were supported in part by RFFI grant 96-02-17113. Also, the research described here was made possible in part by grant RP1-173 of the US Civilian Research and Development Foundation for the Independent States of the Former Soviet Union. The work of R. V. E. L. was also supported in part by NASA grant NAG 5 6311.

REFERENCES

- Bisnovaty-Kogan, G. S. 1993, in *Stellar Jets and Bipolar Outflows*, ed. L. Errico & A. A. Vittone (Dordrecht: Kluwer), 369
- Blandford, R. D., & Payne, D. G. 1982, *MNRAS*, 199, 883
- Bogovalov, S. B. 1997, *A&A*, 323, 634
- Brio, M., & Wu, C. C. 1988, *J. Comput. Phys.*, 75, 400
- Cao, X., & Spruit, H. C. 1994, *A&A*, 287, 80
- Chandrasekhar, S. 1956, *ApJ*, 124, 232
- Contopoulos, J. 1995, *ApJ*, 450, 616
- Contopoulos, J., & Lovelace, R. V. E. 1994, *ApJ*, 429, 139
- Frank, A., & Mellema, G. 1996, *ApJ*, 472, 684
- Heinemann, M., & Olbert, S. 1978, *J. Geophys. Res.*, 83, 2457
- Heyvaerts, J., & Norman, C. A. 1989, *ApJ*, 347, 1055
- Koldoba, A. V., Kuznetsov, O. A., & Ustyugova, G. V. 1992, *Rep. Keldysh Inst. Applied Math. Russian Acad. Science* 69
- Koldoba, A. V., & Ustyugova, G. V. 1994, *Rep. Keldysh Inst. Applied Math. Russian Acad. Science* 87
- Koldoba, A. V., Ustyugova, G. V., Romanova, M. M., Chechetkin, V. M., & Lovelace, R. V. E. 1995, *Ap&SS*, 232, 241
- Königl, A., & Ruden, S. P. 1993, in *Protostars and Planets III*, ed. E. H. Levy & J. Lunine (Tucson: Univ. Arizona), 641
- Koupelis, T., & Van Horn, H. M. 1989, *ApJ*, 342, 146
- Kudoh, T., & Shibata, K. 1995, *ApJ*, 452, L41
- . 1997a, *ApJ*, 474, 362
- . 1997b, *ApJ*, 476, 632
- Kulikovskiy, A. G., & Lyubimov, G. A. 1962, *Magnetic Hydrodynamics*, (Moscow: PhysMatGiz; in Russian)
- Livio, M. 1997, in *ASP Conf. Proc. 121, Accretion Phenomena and Related Outflows*, ed. G. Bicknell, L. Ferrario, & D. Wickramasinghe (San Francisco: ASP), 845
- Lovelace, R. V. E., Berk, H. L., & Contopoulos, J. 1991, *ApJ*, 379, 696
- Lovelace, R. V. E., Mehanian, C., Mobarri, C. M., & Sulkanen, M. E. 1986, *ApJS*, 62, 1
- Lovelace, R. V. E., Newman, W. I., & Romanova, M. M. 1997, *ApJ*, 484, 628
- Lovelace, R. V. E., Romanova, M. M., & Bisnovaty-Kogan, G. S. 1995, *MNRAS*, 275, 244
- Lovelace, R. V. E., Romanova, M. M., & Contopoulos, J. 1993, *ApJ*, 403, 158
- Lovelace, R. V. E., Romanova, M. M., & Newman, W. I. 1994, *ApJ*, 437, 136
- Matsumoto, R., Uchida, Y., Hirose, S., Shibata, K., Hayashi, M. R., Ferrari, A., Bodo, G., & Norman, C. 1996, *ApJ*, 461, 115
- Meier, D. L., Edgington, S., Godon, P., Payne, D. G., & Lind, K. R. 1997, *Nature*, 388, 350
- Mellema, G., & Frank, A. 1998, *MNRAS*, in press
- Mestel, L. 1961, *MNRAS*, 122, 473
- . 1968, *MNRAS*, 138, 359
- Ostriker, E. C. 1997, *ApJ*, 486, 291
- Ouyed, R., & Pudritz, R. E. 1997, *ApJ*, 482, 712
- Ouyed, R., Pudritz, R. E., & Stone, J. M. 1996, *Nature*, 385, 409
- Pelletier, G., & Pudritz, R. E. 1992, *ApJ*, 394, 117
- Polovin, R. V., & Demutskii, V. P. 1990, *Fundamentals of Magnetohydrodynamics* (New York: Consultants Bureau)
- Pudritz, R. E., & Norman, C. A. 1986, *ApJ*, 301, 571
- Roe, P. L. 1986, *Ann. Rev. Fluid Mech.*, 18, 337
- Romanova, M. M., Ustyugova, G. V., Koldoba, A. V., Chechetkin, V. M., & Lovelace, R. V. E. 1997, *ApJ*, 482, 708
- . 1998, *ApJ*, 500, 703
- Ryu, D., Jones, T. W., & Frank, A. 1995, *ApJ*, 252, 785
- Sakurai, T. 1985, *A&A*, 152, 121
- . 1987, *PASJ*, 39, 821
- Shibata, K., & Uchida, Y. 1986, *PASJ*, 38, 631
- Stone, J. M., & Norman, M. L. 1994, *ApJ*, 433, 746
- Uchida, Y., & Shibata, K. 1985, *PASJ*, 37, 515
- Ustyugova, G. V., Koldoba, A. V., Romanova, M. M., Chechetkin, V. M., & Lovelace, R. V. E. 1995, *ApJ*, 439, L39
- Weber, E. J., & Davis, L. 1967, *ApJ*, 148, 217
- Woltjer, L. 1959, *ApJ*, 130, 405